Accepted Manuscript

Evaluating the Height of Biomass Burning Smoke Aerosols Retrieved from Synergistic Use of Multiple Satellite Sensors over Southeast Asia

Jaehwa Lee, N. Christina Hsu, Corey Bettenhausen, Andrew M. Sayer, Colin J. Seftor, Myeong-Jae Jeong, Si-Chee Tsay, Ellsworth J. Welton, Sheng-Hsiang Wang, Wei-Nai Chen

ID: AAQR-15-08-SISEASIA-0506

DOI: 10.4209/aaqr.2015.08.0506

Received Date: 17 August, 2015

Revised Date: 21 December, 2015

Accepted Date: 6 January, 2016

1 Satellite retrievals of aerosol SSA and height are performed over Southeast Asia
2 Retrieval results are compared to data from spaceborne and ground-based instruments
3 Satellite-retrieved SSA and height show promising performance

*Corresponding author. Tel: 1-301-614-6407; Fax: 1-301-614-6307
E-mail address: jaehwa.lee@nasa.gov

Evaluating the height of biomass burning smoke aerosols retrieved from synergistic use of multiple satellite sensors over Southeast Asia

Jaehwa Lee[1,2,*], N. Christina Hsu[1], Corey Bettenhausen[1,3], Andrew M. Sayer[1,4], Colin J. Seftor[1,3], Myeong-Jae Jeong[5], Si-Chee Tsay[1], Ellsworth J. Welton[1], Sheng-Hsiang Wang[6], and Wei-Nai Chen[7]

[1]NASA Goddard Space Flight Center, Greenbelt, MD, USA
[2]Earth System Science Interdisciplinary Center, University of Maryland, College Park, MD, USA
[3]Science Systems & Applications, Inc., Lanham, MD, USA
[4]Goddard Earth Science Technology and Research, Universities Space Research Association, Columbia, MD, USA
[5]Department of Atmospheric and Environmental Sciences, Gangneung-Wonju National University, Gangneung, Gangwon, South Korea
[6]Department of Atmospheric Sciences, National Central University, Chung-Li, Taiwan
[7]Research Center for Environmental Changes, Academia Sinica, Taipei, Taiwan

Abstract

This study evaluates the height of biomass burning smoke aerosols retrieved from a combined use of Visible Infrared Imaging Radiometer Suite (VIIRS), Ozone Mapping and Profiler Suite (OMPS), and Cloud-Aerosol Lidar with Orthogonal Polarization (CALIOP) observations. The retrieved heights are compared against spaceborne and ground-based lidar measurements during the peak biomass burning season (March and April) over Southeast Asia from 2013 to 2015. Based on the comparison against CALIOP, a quality assurance (QA) procedure is developed. It is found that 74% (81-84%) of the retrieved heights fall within 1 km of CALIOP observations for unfiltered (QA-filtered) data, with root-mean-square error (RMSE) of 1.1 km (0.8-1.0 km). Eliminating the requirement of CALIOP observations from the retrieval process significantly increases the temporal coverage with only a slight decrease in the retrieval accuracy; for best QA data, 64% of data fall within 1 km of CALIOP observations with RMSE of 1.1 km. When compared with Micro-Pulse Lidar Network (MPLNET) measurements deployed at Doi Ang Khang, Thailand, the retrieved heights show RMSE of 1.7 km (1.1 km) for unfiltered (QA-filtered) data for the complete algorithm, and 0.9 km (0.8 km) for the simplified algorithm.

Keywords: aerosol height, satellite, biomass burning, Southeast Asia, 7-SEAS

[*]Corresponding author. Tel: 1-301-614-6407; Fax: 1-301-614-6307
E-mail address: jaehwa.lee@nasa.gov

INTRODUCTION

Aerosol height has been recognized as an important parameter in the determination of the Earth's energy budget. Through scattering and absorption of radiation, aerosols can modulate the radiation field, and thus heating rate, at different vertical levels of the atmosphere (Hansen *et al.*, 1997; Podgorny and Ramanathan, 2001). Aerosol-cloud interactions, crucial elements in climate forcing, are also dependent on aerosol altitude (Rosenfeld *et al.*, 2014). Height information has implications for air quality issues, as it is a key parameter in deriving surface-level aerosol concentrations from more easily accessible total column aerosol optical depth (AOD) measurements from ground-based or spaceborne remote sensing instruments (van Donkelaar *et al.*, 2006). In addition, an independent data set can contribute to providing chemistry transport models with injection height information for air quality predictions, and serve as an evaluation target for the model results (e.g. Kahn *et al.*, 2007; Koffi *et al.*, 2012).

There has been increasing interest in the synergistic use of multiple satellite sensors to address aerosol-related scientific problems (e.g. Anderson *et al.*, 2005; Jeong and Li, 2005; Kim *et al.*, 2007; Torres *et al.*, 2013). The Aerosol Single-scattering albedo and Height Estimation (ASHE) algorithm (Jeong and Hsu, 2008; Lee *et al.*, 2015) is one such effort, among others (e.g. Satheesh *et al.*, 2009), to retrieve the height of UV-absorbing aerosols (e.g. smoke and dust) over broad areas. The algorithm takes advantage of Visible Infrared Imaging Radiometer Suite (VIIRS),

Ozone Mapping and Profiler Suite (OMPS), and Cloud-Aerosol Lidar with Orthogonal Polarization (CALIOP) observations to simultaneously retrieve a representative single-scattering albedo (SSA) and spatially resolved aerosol height over the entire VIIRS/OMPS granule. The Moderate Resolution Imaging Spectroradiometer (MODIS) and Ozone Monitoring Instrument (OMI) can be used in place of VIIRS and OMPS, respectively, as the sensor characteristics of MODIS/OMI are similar to VIIRS/OMPS.

Other satellite sensors, notably the Multi-Angle Imaging SpectroRadiometer (MISR) and (Advanced) Along-Track Scanning Radiometers ((A)ATSR), can also provide aerosol heights using multi-angle imaging (i.e., parallax) (Nelson *et al.*, 2013; Fisher *et al.*, 2014). However, with the ability to retrieve data over a much broader spatial domain (thousands of kilometres in the case of MODIS and VIIRS) including aerosol layers far from the source region, ASHE retrievals can complement the existing data sets (Note the multi-angle approach is limited to aerosol plumes that have discernible features, i.e. typically close to their sources; Kahn *et al.*, 2008).

Our previous studies (Jeong and Hsu, 2008; Lee *et al.*, 2015) showed promising results when retrieving heights for rather heavy smoke and dust cases; Jeong and Hsu (2008) reported the coefficient of determination of 0.86 between ASHE-retrieved and CALIOP-derived aerosol heights for retrievals for 10 MODIS granules over North America and Southeast Asia; Lee *et al.* (2015) reported root-mean-square errors (RMSEs) generally less than 1 km for single-layered

smoke and dust aerosol events. However, the evaluation was solely based on CALIOP data. Because the ASHE algorithm makes use of CALIOP aerosol heights to derive SSA along the CALIOP track, it was difficult to evaluate the performance of ASHE over parts of the granule far from the CALIOP track, where variability in the SSA (assumed constant across the MODIS/VIIRS granules) could lead to error in retrieved aerosol heights. In addition, the number of samples available was insufficient to develop a robust understanding of error characteristics, which hindered attempts to create a quality assurance (QA) procedure to help guide users to an appropriate subset of the data for scientific applications.

Thus, this study aims to further evaluate the ASHE products (SSA and aerosol height) to better understand their error characteristics. We base the present study on data from the Seven Southeast Asian Studies/Biomass-burning Aerosols & Stratocumulus Environment: Lifecycles and Interactions Experiment (7-SEAS/BASELInE), which was conducted over Southeast Asia during spring season (March and April) from 2013 to 2015 (and onwards) (cf. Lin *et al.*, 2013; Reid *et al.*, 2013; Tsay *et al.*, 2013). The frequent smoke aerosols over the study domain and abundant ground-based observations during this field campaign provided a testbed on which the ASHE products can thoroughly be examined over a longer period of time than previous studies.

DATA

92

93 ASHE retrievals were performed over Southeast Asia (8°N-28°N, 90°E-110°E) during the
94 peak biomass burning season (March and April) from 2013 to 2015. The retrieved heights of
95 biomass burning smoke aerosols were compared against CALIOP and ground-based Micro Pulse
96 Lidar Network (MPLNET; Welton *et al.*, 2001) measurements deployed at Doi Ang Khang,
97 Thailand as part of 7-SEAS/BASELInE. Aerosol Robotic Network (AERONET; Holben *et al.*,
98 1998) inversion data (Dubovik and King, 2000; Dubovik *et al.*, 2006) were also used to evaluate
99 the SSA retrievals at six locations where the smoke aerosols were frequently observed. Fig. 1
100 shows the distribution of the ground-based instruments under the typical pathway of biomass
101 burning smoke aerosols within the study domain (Tsay *et al.*, 2013). Table 1 summarizes the site
102 information.

103 The MPLNET Micro Pulse Lidar (MPL) (Campbell *et al.*, 2002), mounted on NASA's
104 Surface-sensing Measurements for Atmospheric Radiative Transfer (SMART) mobile facility
105 (Tsay *et al.*, 2013), utilizes a short pulse, eye-safe laser at 532 nm to provide vertical profiles of
106 aerosol extinction and backscatter coefficients by using the laser signal that was backscattered by
107 atmospheric constituents (air molecules, aerosols, and clouds). The columnar AOD measured by
108 the collocated AERONET Sun/sky radiometer constrains the ill-posed lidar equation to derive the
109 lidar ratio (extinction-to-backscatter ratio) and retrieve the extinction profile (Welton *et al.*, 2000,

2002). For MPLNET and ASHE comparisons, we use the gridded level 1.5a aerosol total backscatter coefficient (TBC) profiles with a vertical resolution of 75 m and a temporal resolution of 20 min. The MPLNET aerosol height to be compared is determined as the aerosol top height after removing the integrated TBC of 0.024 km^{-1} sr^{-1} from the top portion of the profile, to avoid potential errors caused by thin elevated aerosol layers above the layer of interest (cf. Lee *et al.*, 2015).

Comparison of spatially resolved satellite data with temporally resolved point measurements has conventionally been performed with spatial and temporal statistics for satellite and points measurements, respectively. This is to resolve the different sampling characteristics of the data sets and increase the number of data points, which is critical for statistical significance of the comparison. For aerosol studies, a spatial window of 25 km from the point measurement and a temporal window of 30 min from the satellite overpass time have widely been used (e.g. Ichoku *et al.*, 2002). However, the coarse spatial resolution of the ASHE product (50 km × 50 km at nadir) did not allow us to use this spatial criterion since it would be difficult to get collocated samples between ASHE and MPLNET, particularly near the edge of the swath where the pixel size is enlarged. Ichoku *et al.* (2002) reported using MODIS data that mean AOD showed similar statistics for spatial windows ranging from 30 × 30 km to 90 × 90 km (which corresponds to spatial windows of approximately 15-45 km for the convention used here) over various locations.

Based on previous work and the fact that the spatial variability of ATH is generally lower than that of AOD (often factor of two or more lower in terms of relative standard deviation over the study area because of its dependence on large-scale dynamics such as boundary layer height), we used a relaxed spatial window of 50 km and temporal window of 30 min for comparison between ASHE and MPLNET heights. This almost doubled the number of data points as compared to the spatial window of 25 km, while improving the comparison statistics.

For AERONET, the cloud-screened (but not quality-assured) Level 1.5 inversion product, which provides SSA at 440, 675, 870, and 1020 nm, were used, as the quality-assured Level 2.0 product only provided a limited number of samples for comparison (the number of collocated Level 1.5 inversions within 3 h of ASHE were about a factor of three larger than that of Level 2.0, when the filters described below were applied). However, the data are used only if the 440 nm AOD is higher than 0.4, 440-870 nm AE higher than 1.5, and solar zenith angle (SZA) higher than 40^{o} to reduce the level of uncertainty. We use a SZA threshold of 40° instead of Level 2.0's 50° because SZA was the main reason for the small number of collocations when Level 2.0 data was used. It is known that the AERONET-retrieved SSA has a retrieval uncertainty of 0.03 for 440 nm AOD > 0.4 and SZA > 50° (Dubovik *et al.*, 2000; Holben *et al.*, 2006), which is expected to decrease with increasing AOD. Since the smoke events on which this study focuses generally show 440 nm AOD higher than 0.4, and the SSA error is dependent on the air mass (which is

146 related to both AOD and SZA) and range of scattering angles sampled, the uncertainty of SSA is
147 expected to be similar or lower than 0.03 for some severe cases despite the relaxed SZA threshold.
148 Note that given the aforementioned filters applied to the Level 1.5 data set and calibration just
149 before the field experiment every year for most of AERONET instruments used, the difference of
150 retrieval accuracy resulting from AERONET Sun photometer calibration uncertainty between the
151 two data sets is expected to be small.

152 Both temporal and spatial constraints were applied to the comparison of SSA between ASHE
153 and AERONET. First, the AERONET data within 3 h of the VIIRS/OMPS overpass time were
154 averaged at each site. Then the mean of these averaged SSA at AERONET sites located within 50
155 km of smoke layers detected by ASHE (i.e., 550 nm AOD > 0.3 and UV aerosol index; UVAI >
156 0.7) were calculated and used for comparison.

157

158 ## ASHE ALGORITHM

159

160 This section briefly describes the ASHE algorithm as applied to VIIRS, OMPS, and CALIOP
161 observations; a more detailed description can be found in Jeong and Hsu (2008) and Lee *et al.*
162 (2015). Note VIIRS/OMPS and CALIOP are aboard the Suomi National Polar-orbiting
163 Partnership (S-NPP) and Cloud-Aerosol Lidar and Infrared Pathfinder Satellite Observations

(CALIPSO), respectively. In principle, the algorithm utilizes the sensitivity of UVAI to AOD, SSA, and height of UV-absorbing aerosols (cf. Hsu *et al.*, 1999). As shown in the flowchart (Fig. 2), the algorithm utilizes four kinds of aerosol products in its retrieval process: AOD and AE from VIIRS, UVAI from OMPS, and the TBC profile from CALIOP. After collocating the various aerosol products from each sensor, the algorithm detects UV-absorbing aerosols (smoke or dust) by a combined use of UVAI and Ångström exponent (AE). If the VIIRS/OMPS granule includes UV-absorbing aerosols, and CALIOP provides the height of these aerosols, the algorithm first retrieves SSA for each VIIRS/OMPS/CALIOP collocated pixel. This is done by using the sensitivity of UVAI to SSA given AOD and aerosol height provided by VIIRS and CALIOP, respectively. To extent the height retrieval away from the narrow CALIOP track, the median SSA is chosen to represent the entire smoke or dust layer in the VIIRS/OMPS granule, and used to retrieve aerosol height using the UVAI sensitivity to aerosol height given AOD and SSA. The algorithm can be applied without CALIOP observations if SSA is provided from other data sources, which will be referred to as 'simplified' algorithm as compared to the 'complete' algorithm. Note the smoke and dust pixels are processed separately using appropriate aerosol optical models.

The retrieved height is considered as the aerosol top height (ATH) if the system is single-layered, or as the radiatively-effective height in the case of multiple layers separated clearly from

one another. The SSA can be propagated from the UV to other wavelengths using the assumed aerosol model. Currently, the SSA is provided at 340, 378, 412, 445, 488, 555, and 672 nm (OMPS or VIIRS bands) for potential use as input for OMPS and/or VIIRS aerosol retrieval algorithms. In this application, we only assume smoke aerosol models since smoke (as opposed to dust) dominates during the spring season over the study domain (Lee *et al.*, 2010).

The VIIRS aerosol product is created using the VIIRS Deep Blue algorithm, which is based on the Collection 6 (C6) MODIS Deep Blue algorithm (Hsu *et al.*, 2013; Sayer *et al.*, 2013, 2014b), and optimized for the slightly different VIIRS sensor. The aerosol product provides daily global coverage at a spatial resolution of 6 km × 6 km at nadir with a swath of 3040 km.

For UVAI, the 340-378 nm wavelength pair of OMPS measurements, which is not affected by ozone absorption, is used and provides data at a spatial resolution of 50 km × 50 km at nadir (Seftor *et al.*, 2014). The VIIRS data are aggregated to match the OMPS resolution in the retrieval process, and the retrieved values are provided at the OMPS spatial resolution with a swath of 2800 km.

The CALIOP aerosol height is determined from the aerosol TBC product at 5 km resolution using the same approach as used for MPLNET, except with a TBC threshold of 0.03 km^{-1} sr^{-1} to account for the difference in the vertical resolutions between the two instruments (60 m for CALIOP vs. and 75 m for MPLNET). Note the vertical resolution of the CALIOP's aerosol

profile product changes to 180 m at an altitude of 20.2 km and higher, whereas the MPLNET's does not change throughout the entire vertical range. The CALIOP-derived height in addition to TBC profile itself is used to determine the representative profile shape of the aerosol layer of interest, which is an input to the present algorithm (see Lee *et al.*, 2015 for details), as well as used to evaluate the retrieval product.

Fig. 3 shows an example of ASHE retrievals for a smoke event observed over the Indochina Peninsula on 29 March 2013, and comparisons of the retrieved ATH against CALIOP- and MPLNET-derived values and the retrieved SSA against AERONET inversion data. In this region, smoke aerosols originate from scattered burning sources as seen by the MODIS fire mask (Giglio *et al.*, 2003), which makes their optical and microphysical properties complicated. Smoke properties can vary according to material burned, combustion type, and aging processes (e.g. Dubovik *et al.*, 2002; Reid *et al.*, 2005; Lee *et al.*, 2010; Sayer *et al.*, 2014a). For the test case, the smoke layer with AOD generally higher than 0.8 (not shown) resides at altitudes ranging from 2-5 km (Fig. 3(b)). The ASHE ATH shows a high level of correspondence compared to the CALIOP observations, with a root-mean-square error (RMSE) of 0.5 km and mean bias (MB) of 0.2 km (Fig. 3(c)). The comparison with MPLNET data at Doi Ang Khang (Fig. 3(d)) also reveals a remarkable consistency between the two independent data, mainly due to the high accuracy of the retrieved SSA (0.89 for ASHE vs. 0.90 for AERONET as shown in Fig. 3(e)).

SIMPLIFIED ALGORITHM

As described above, the ASHE algorithm can be applied without CALIOP observations if the SSA is provided by other data sources. By eliminating the requirement of CALIOP observations, which limits the application of this algorithm to only those granules where CALIOP's narrow track passes through the aerosol layer of interest, a significant increase in the spatiotemporal coverage can be achieved. Here, we focus on the use of climatological SSA data derived from the ASHE retrievals, although the climatology can be created using any data sources that provide SSA. The ASHE-derived one has an advantage in that it provides consistency with the aerosol models assumed in the algorithm.

Fig. 4 shows frequency distributions of 440 nm (AERONET) or 445 nm (ASHE) SSA retrieved over the study domain for the six-month period (March and April, 2013-2015). For AERONET, daily mean SSA values from the six individual sites are included, which are calculated for 440 nm AOD > 0.4 and AE > 1.5 to represent smoke aerosols. Some differences are found between the two data sets; for instance, ASHE-retrieved values show narrower distribution and lower frequency in low SSA values (~0.85) than that of AERONET. However, the two data sets resemble each other as with both show mean and median SSA of 0.89 and a

standard deviation of 0.03 for ASHE and 0.033 for AERONET. The differences are due to the difference in the number of samples (59 for ASHE vs. 503 for AERONET), the fixed aerosol models used in retrieving SSA in the ASHE algorithm, and retrieval uncertainty. The theoretical uncertainty estimates reported in Lee *et al.* (2015) suggested that the SSA error of 0.03 corresponded to positive ATH error of 50% when overestimated and negative error of 25% when underestimated for smoke aerosols with AOD of 1.0 and ATH of 5 km. Based on the histogram analysis, a fixed SSA of 0.89 is used in the simplified algorithm to be applied without CALIOP observations over the study domain.

EVALUATION RESULTS

Comparison to CALIOP and development of QA procedure

Despite the caveats of using CALIOP data in evaluating the retrieved ATH (used as input for SSA retrievals and spatial proximity), CALIOP still remains an important source of validation data due to the large number of samples. Moreover, the variability in smoke properties along the CALIOP track resulting from the complex burning sources over Southeast Asia can represent the spatial variability of SSA within a VIIRS/OMPS granule to some extent (although the variability along the CALIOP track could be smaller than that over the VIIRS/OMPS granule). Here, the

254 retrieved ATH from the complete algorithm is compared to the CALIOP-derived values, and a
255 QA procedure is developed based on the comparison results.

256 Fig. 5 shows RMSE of ASHE-retrieved ATH as compared to the CALIOP-derived values as a
257 function of thresholds for three different QA filters that can affect the retrieval accuracy. A
258 nearest-neighbor approach is used for the comparison. A thorough analysis of the retrieval results
259 reveals that the accuracy of ATH depends on various factors, including number of pixels
260 discarded at the edge of the VIIRS/OMPS swath (removing effects of increased pixel size at high
261 scan angles), number of collocations between VIIRS/OMPS and CALIOP for SSA retrievals, and
262 spatial co-variability of UVAI and AOD (hereafter referred to as 'edge-of-swath', 'number-of-
263 collocation', and 'spatial variability' filters, respectively). The comparison results reveal that the
264 RMSE of the unfiltered data is ~1.1 km, decreasing with stricter thresholds for the QA filters
265 until the number of data points plays a significant role. Here, the thresholds are determined as the
266 point where the decrease in RMSE slows down but at least 50% of data points are retained.
267 However, in an operational setting, QA procedures usually incorporate visual inspection of a
268 more extensive data record once generated, so these thresholds may change in the future
269 (although the procedure will be based on the same philosophy).

270 The increase in pixel size of OMPS with scan angle means more probable subpixel cloud
271 contamination or scene heterogeneity in the pixels far from nadir than those near nadir. Cloud

contamination has detrimental effects on both SSA and ATH retrievals since it changes the UVAI, and the present algorithm assumes clear-sky for UVAI calculations. The effect on SSA (and ATH retrieved using a wrong assumption about SSA) is potentially more significant than the direct effect on ATH because SSA is the largest source of error, and the error can propagate over the entire granule. In addition, when the collocation between VIIRS/OMPS and CALIOP for SSA retrievals occurs at the edge of the VIIRS/OMPS swath, the temporal difference between the two satellites (S-NPP and CALIPSO) can be as large as 60 min (because the two satellites have the same daytime local equatorial crossing time of ~13:30, and the satellites are passing different time zones). The large temporal difference can cause the two satellites to observe inconsistent heights of fast-changing aerosol layers. As a result, the procedure to retrieve SSA is bypassed when the collocation is made in the three farthest VIIRS/OMPS pixels from nadir in both cross-track directions.

The number of collocations between VIIRS/OMPS and CALIOP can affect the retrieval accuracy of SSA. Although some of the error in the Deep Blue AOD are contextual (i.e. depend on geometry, AOD, and aerosol/surface type; Sayer *et al.,* 2013), increasing the number of points should decrease the AOD error. Thus, theoretically, the retrieved SSA (retrieved by constraining AOD and aerosol height) should asymptotically approach a true value as the number of collocations increases, if the input aerosol profile from CALIOP and assumed aerosol model in

290 the retrieval process are accurate. As a result, a threshold of a minimum of 30 points is used for
291 the number-of-collocation filter.

292 While the aforementioned parameters affect the retrieval accuracy through SSA, some errors
293 are associated with pixel-level uncertainties. As shown in Lee *et al.* (2015) the ATH uncertainty
294 depends on cloud contamination and AOD. The spatial variability filter (defined as relative
295 standard deviation of the ratio between UVAI and AOD over the consecutive 3 × 3 pixels) is a
296 useful metric to determine whether the two error sources play significant roles. A threshold of 1.0
297 is chosen for the spatial variability filter together with an AOD threshold of 0.5 for the final test.
298 Note that data with the relative standard deviation lower than the threshold pass the QA test,
299 while the other filters work the other way around.

300 Fig. 6 shows scatterplots between CALIOP-derived and ASHE-retrieved ATHs for different
301 QA filters and corresponding SSA (used for the ATH retrievals compared) comparisons between
302 AERONET and ASHE. When comparing the scatterplots and comparison statistics of ATH and
303 SSA between data with and without QA filters, it is found that the edge-of-swath filter effectively
304 removes outliers in both ATH and SSA; the fraction of ASHE-retrieved ATH within 1 km of
305 CALIOP values improves from 73% to 81% and the fraction of ASHE-retrieved SSA within 0.03
306 of AERONET inversions increases from 63% to 73%. Including the number-of-collocation filter
307 on top of the edge-of-swath filter further improves the retrieval accuracy, particularly for SSA

(fraction within 0.03 of AERONET inversions increases from 73% to 88%). The spatial variability and AOD filters further remove some of the outliers in the retrieved ATH, resulting in 75% (97%) of data falling within 1 km (1.5 km) of CALIOP-derived values (not shown because the filters do not affect SSA retrieval accuracy).

For the complete algorithm, data without any QA filters, that passed through the edge-of-swath filter, and that passed through all of the QA filters will be referred to as 'unfiltered', 'all QA', and 'best QA' data, respectively. For the simplified algorithm, since it does not include the procedure to retrieve SSA (so that the edge-of-swath and number-of-collocation filters do not affect the retrieval process), data without any filters will be referred to as 'all QA' data, while the data which passes through the spatial variability and AOD filters will be 'best QA' data.

Table 2 summarizes the comparison statistics between ASHE and CALIOP ATHs. Results for different algorithm types and QA filters are presented. For the complete algorithm, the ATH shows RMSE ranging from 0.8-1.1 km, decreasing with the level of QA as intended. In RMSE metric there is only a slight difference between unfiltered and QA-filtered data. However, the reduced number of data points (from 627 to 335 or 177) and increased fraction within 1 km (from 74% to 81 or 84%) when applying the QA filters imply that the unfiltered data includes a large number of outliers, mainly due to the large uncertainty in the retrieved SSA and cloud contamination in the enlarged pixels near the edge of the swath (note that the difference between

unfiltered and QA-filtered data is whether using SSA retrieved at the edge of swath). The RMSEs of the QA-filtered data correspond to 30-40% uncertainty given a mean height of ~3 km, consistent with the theoretical uncertainty in Lee *et al.* (2015).

The simplified algorithm shows slightly reduced performance in terms of RMSE, but has a larger number of data points than the complete algorithm. However, fairly large decreases are observed in the fractions within 1 km metric for both all QA and best QA data, which suggests that the simplified algorithm is more suitable for climatological studies rather than those requiring more accurate instantaneous information (such as air quality monitoring).

Comparison to MPLNET data

Fig. 7 shows time series of ASHE-retrieved best QA ATH and MPLNET-derived ATHs for March and April from 2013 to 2014. Time series of AOD and SSA are also shown to aid in the analysis of the error characteristics. The height of biomass burning smoke aerosols over the region is generally 2-5 km, with strong (~2 km) diurnal variability for certain days. The smoke layers are sometimes observed at higher altitudes, likely due to high radiant power of the fire and/or high boundary layer height.

The bias in the retrieved ATH is a function of biases in AOD and SSA. Because UVAI increases with increasing ATH, increasing AOD, and decreasing SSA (cf. Hsu *et al.*, 1999; Ginoux and Torres, 2003), for a given UVAI, high biases in AOD and SSA result in low bias and

high bias in ATH, respectively; the converse is true for low biases. The errors due to AOD and SSA sometimes cancel out, but a large bias can also arise when the biases in AOD and SSA are in opposite directions to each other, so that the resulting ATH errors combine. A strong underestimation observed on 2 March 2013 is found to be due to the strong negative bias in SSA. Although the low bias in AOD is expected to cancel some of the error caused from the low bias in SSA, the resulting ATH is still strongly biased low, because ATH is more sensitive to errors in SSA than AOD. The biases in ATH can be explained by errors in AOD and SSA in general. However, it is difficult to confine the source of error when other parameters play a significant role, such as aerosol model assumption in ASHE, SSA retrieval uncertainty in AERONET, etc.

It is noteworthy that the simplified algorithm performs fairly well with a fixed SSA, even though the variability of SSA can be quite large (as seen by AERONET). The SSA at Doi Ang Khang tends to increase from March to April, possibly due to changes in atmospheric conditions such as relative humidity, and aging of the smoke aerosols. This implies that time- or atmospheric condition-dependent SSA parameterization in addition to the mean state could potentially improve the simplified algorithm, although it is beyond the scope of this study to include such effects in the algorithm.

Table 3 summarizes the comparison statistics against MPLNET data. The statistics generally show tendency similar to the one seen for comparisons against CALIOP, i.e., increasing

362 performance with the level of QA (except for the best QA data from complete algorithm due to
363 the limited number of samples). However, in this case the simplified algorithm shows slightly
364 better performance than the complete algorithm in terms of RMSE. The opposite was true for the
365 comparison against CALIOP. For the complete algorithm, the fraction of QA-filtered data within
366 1 km of MPLNET's decreases as compared to the case against CALIOP (81-84% for CALIOP vs.
367 71-77% for MPLNET), whereas it increases (61-64% for CALIOP vs. 70-75% for MPLNET) for
368 the simplified algorithm. Accordingly, RMSE increases from 0.8-1.0 km (CALIOP) to 1.1 km
369 (MPLNET) for the complete algorithm, and decreases from 1.1-1.2 km (CALIOP) to 0.8-0.9 km
370 (MPLNET) for the simplified algorithm. Although the poorer performance of the complete
371 algorithm than the simplified one when comparing to MPLNET is likely due to a sampling issue
372 (only 13 data points for all QA data, and 7 for best QA data), the assumption of uniform SSA is
373 thought to affect the retrieval accuracy to some extent. Note Student's t-test did not show a
374 significant difference in error distributions between the complete and simplified algorithm at a
375 95% confidence level.
376

377 ## SUMMARY AND CONCLUSIONS

378

379 This study assessed the ASHE algorithm in retrieving the height of biomass burning smoke
380 aerosols by comparing to spaceborne and ground-based lidar measurements during the peak

burning season over Southeast Asia. We determined that the performance of the algorithm depends on uncertainty in the retrieved SSA, representation of the SSA within a granule, and pixel-level uncertainties in AOD and UVAI. In particular, the SSA retrieved along the edge of the VIIRS/OMPS swath showed large uncertainty and limited the performance of the algorithm. When compared with CALIOP data, the retrieved height showed uncertainty of 30-40% depending on algorithm type (complete vs. simplified) and validation target (CALIOP vs. MPLNET), given a mean smoke height of ~3 km over the study domain. The complete algorithm generally showed better performance than the simplified algorithm as it uses retrieved SSA and CALIOP-derived profile shape in its processing stream while assumed values are used for the simplified algorithm. However, when compared with MPLNET data, the opposite was observed, suggesting that a longer-term evaluation is required to better understand the error characteristics at locations far from where the SSA is retrieved.

As the requirement for CALIOP observations is the largest limitation in achieving more complete global coverage, efforts will be made to create a global SSA map of UV-absorbing aerosols. The similar frequency distributions of SSA between ASHE and AERONET suggest possible use of the AERONET-derived SSA climatology, in particular over land, which is much easier to achieve than using ASHE given the computational expense required for the global

398 processing of ASHE. The simplified algorithm will provide users with more options for their
399 respective science questions, depending on requirements on accuracy vs. frequency of data.
400 Although improved since its development, the algorithm still has room for further
401 enhancement. First of all, the aerosol layer for which the SSA is retrieved can be separated from
402 the others within a granule, such that the algorithm can be only applied to the aerosol layer of
403 interest. Because a poor assumption about SSA is the largest potential source of error, the
404 procedure would improve the quality of ATH further, at the cost of reduced spatial coverage. In
405 addition, a more complete suite of aerosol models as functions of size distributions and absorbing
406 AE is required to further reduce errors resulting from aerosol model assumptions. The VIIRS-
407 retrieved size information, such as AE and fine-mode AOD fraction, can help to constrain the
408 size information, in particular over ocean where size information is more reliable than over land.
409 Meanwhile, the spectral absorption characteristics can be constrained by climatological data
410 derived from AERONET (e.g. Sayer *et al.*, 2014a) or other sources.
411 With the current and planned new missions carrying spaceborne lidars, such as the Cloud-
412 Aerosol Transport System (CATS), Earth Clouds, Aerosols and Radiation Explorer (EarthCARE),
413 and Aerosol-Cloud-Ecosystems (ACE), the synergistic use of multiple satellite sensors will be
414 refined further to provide more complete information about aerosol height over the globe.
415

ACKNOWLEDGMENTS

This project is funded by the NASA Earth Observing System program, managed by H. Maring, and the NASA Micro-Pulse Lidar Network by the NASA Earth Observing System and Radiation Sciences Program. The VIIRS, OMPS, and CALIOP science teams are gratefully acknowledged for their efforts to create and maintain the data records used in this investigation. We thank the PIs and managers (B. N. Holben, S. Janjai, and N.-H. Lin) for establishing and maintaining the AERONET sites used in this study.

REFERENCES

Anderson, T. L., Charlson, R. J., Bellouin, N., Boucher, O., Chin, M., Christopher, S. A., Haywood, J., Kaufman, Y. J., Kinne, S., Ogren, J. A., Remer, L. A., Takemura, T., Tanré, D., Torres, O., Trepte, C. R., Wielicki, B. A., Winker, D. M. and Yu, H. (2005). An "A-Train" strategy for quantifying direct climate forcing by anthropogenic aerosols. *Bull. Amer. Meteor. Soc.* 86: 1795-1809.

Campbell, J. R., Hlavka, D. L., Welton, E. J., Flynn, C. J., Turner, D. D., Spinhirne, J. D., Scott, V. S. and Hwang, I. H. (2002). Full-time, eye-safe cloud and aerosol lidar observation at

434 atmospheric radiation measurement program sites: Instruments and data processing. *J. Atmos.*
435 *Oceanic Technol.* 19: 431-442.
436 Dubovik, O., Holben, B., Eck, T. F., Smirnov, A., Kaufman, Y. J., King, M. D., Tanré, D. and
437 Slutsker, I. (2002). Variability of absorption and optical properties of key aerosol types
438 observed in worldwide locations. *J. Atmos. Sci.* 59: 590-608.
439 Dubovik, O. and King, M. D. (2000). A flexible inversion algorithm for retrieval of aerosol
440 optical properties from Sun and sky radiance measurements. *J. Geophys. Res. Atmos.* 105:
441 20673-20696.
442 Dubovik, O., Sinyuk, A., Lapyonok, T., Holben, B. N., Mishchenko, M., Yang, P., Eck, T. F.,
443 Volten, H., Muñoz, O., Veihelmann, B., van der Zande, W. J., Leon, J.-F., Sorokin, M. and
444 Slutsker, I. (2006). Application of spheroid models to account for aerosol particle
445 nonsphericity in remote sensing of desert dust. *J. Geophys. Res. Atmos.* 111: D11208.
446 Dubovik, O., Smirnov, A., Holben, B. N., King, M. D., Kaufman, Y. J., Eck, T. F. and Slutsker, I.
447 (2000). Accuracy assessments of aerosol optical properties retrieved from Aerosol Robotic
448 Network (AERONET) Sun and sky radiance measurements. *J. Geophys. Res. Atmos.* 105:
449 9791-9806.

450 Fisher, D., Muller, J.-P. and Yershov, V. N. (2014). Automated stereo retrieval of smoke plume
451 injection heights and retrieval of smoke plume masks from AATSR and their assessment with
452 CALIPSO and MISR. *IEEE Trans. Geosci. Remote Sens.* 52: 1249-1258.
453 Giglio, L., Descloitres, J., Justice, C. O. and Kaufman, Y. J. (2003). An enhanced contextual fire
454 detection algorithm for MODIS. *Remote Sens. Environ.*, 87: 273-282.
455 Ginoux, P. and Torres, O. (2003). Empirical TOMS index for dust aerosol: Applications to model
456 validation and source characterization. *J. Geophys. Res. Atmos.* 108: 4534.
457 Hansen, J., Sato, M. and Ruedy, R. (1997). Radiative forcing and climate response. *J. Geophys.*
458 *Res. Atmos.* 102: 6831–6864.
459 Holben, B. N., Eck, T. F., Slutsker, I., Smirnov, A., Sinyuk, A., Shafer, J., Giles, D. and Dubovik,
460 O. (2006). AERONET's version 2.0 quality assurance criteria. *Proc. SPIE* 6408: 64080Q.
461 Holben, B. N., Eck, T. F., Slutsker, I., Tanré, D., Buis, J. P., Setzer, A., Vermote, E., Reagan, J.
462 A., Kaufman, Y. J., Nakajima, T., Lavenu, F., Jankowiak, I. and Smirnov, A. (1998).
463 AERONET - A federated instrument network and data archive for aerosol characterization.
464 *Remote Sens. Environ.* 66: 1-16.
465 Hsu, N. C., Herman, J. R., Torres, O., Holben, B. N., Tanré, D., Eck, T. F, Smirnov, A., Chatenet,
466 B. and Lavenu, F. (1999). Comparison of the TOMS aerosol index with Sun-photometer
467 aerosol optical thickness: Results and applications. *J. Geophys. Res. Atmos.* 104: 6269-6279.

468 Hsu, N. C., Jeong, M.-J., Bettenhausen, C., Sayer, A. M., Hansell, R., Seftor, C. S., Huang, J. and
469 Tsay, S.-C. (2013). Enhanced Deep Blue aerosol retrieval algorithm: The second generation. *J.*
470 *Geophys. Res. Atmos.* 118: 9296-9315.
471 Ichoku, C., Chu, D. A., Mattoo, S., Kaufman, Y. J., Remer, L. A., Tanré, D., Slutsker I. and
472 Holben, B. N. (2002). A spatio-temporal approach for global validation and analysis of
473 MODIS aerosol products. *Geophys. Res. Lett.* 29:1616.
474 Jeong, M.-J. and Hsu, N. C. (2008). Retrievals of aerosol single-scattering albedo and effective
475 aerosol layer height for biomass-burning smoke: Synergy derived from "A-Train" sensors.
476 *Geophys. Res. Lett.* 35: L24801.
477 Jeong, M.-J. and Li, Z. (2005). Quality, compatibility, and synergy analyses of global aerosol
478 products derived from the advanced very high resolution radiometer and Total Ozone Mapping
479 Spectrometer. *J. Geophys. Res. Atmos.* 110: D10S08.
480 Kahn, R. A., Chen, Y., Nelson, D. L., Leung, F.-Y., Li, Q., Diner, D. J. and Logan, J. A. (2008).
481 Wildfire smoke injection heights: Two perspectives from space. *Geophys. Res. Lett.* 35:
482 L04809.
483 Kahn, R. A., Li, W.-H. Moroney, C., Diner, D. J., Martonchik, J. V. and Fishbein, E. (2007).
484 Aerosol source plume physical characteristics from space-based multiangle imaging. *J.*
485 *Geophys. Res. Atmos.* 112: D11205.

Kim, J., Lee, J., Lee, H. C., Higurashi, A., Takemura, T. and Song, C. H. (2007). Consistency of the aerosol type classification from satellite remote sensing during the Atmospheric Brown Cloud-East Asia Regional Experiment campaign. *J. Geophys. Res. Atmos.* 112: D22S33.

Koffi, B., et al. (2012). Application of the CALIOP layer product to evaluate the vertical distribution of aerosols estimated by global models: AeroCom phase I results. *J. Geophys. Res. Atmos.* 117: D10201.

Lee, J., Hsu, N. C., Bettenhausen, C., Sayer, A. M., Seftor, C. J., and Jeong, M.-J. (2015). Retrieving the height of smoke and dust aerosols by synergistic use of VIIRS, OMPS, and CALIOP observations, *J. Geophys. Res. Atmos*. 120: 8372–8388.

Lee, J., Kim, J., Song, C. H., Kim, S. B., Chun, Y., Sohn, B. J. and Holben, B. N. (2010). Characteristics of aerosol types from AERONET sunphotometer measurements. *Atmos. Environ.* 44: 3110-3117.

Lin, N. et al. (2013). An overview of regional experiments on biomass burning aerosols and related pollutants in Southeast Asia: From BASE-ASIA and the Dongsha Experiment to 7-SEAS. *Atmos. Environ.* 78: 1-19.

Nelson, D. L., Garay, M. J., Kahn, R. A. and Dunst, B. A. (2013). Stereoscopic height and wind retrievals for aerosol plumes with the MISR INteractive eXplorer (MINX). *Remote Sens.* 5: 4593-4628.

504 Podgorny, I. A. and Ramanathan, V. (2001). A modeling study of the direct effect of aerosols
505 over the tropical Indian Ocean. *J. Geophys. Res. Atmos.* 106:24097-24105.
506 Reid, J. S., Eck, T. F., Christopher, S. A., Koppmann, R., Dubovik, O., Eleuterio, D. P., Holben,
507 B. N., Reid, E. A. and Zhang, J. (2005). A review of biomass burning emissions part III:
508 intensive optical properties of biomass burning particles. *Atmos. Chem. Phys.* 5: 827-849.
509 Reid, J. S. et al. (2013). Observing and understanding the Southeast Asian aerosol system by
510 remote sensing: An initial review and analysis for the Seven Southeast Asian Studies (7SEAS)
511 program. *Atmos. Res.* 122: 403-468.
512 Rosenfeld, D., Sherwood, S., Wood, R. and Donner, L. (2014). Climate effects of aerosol-cloud
513 interactions. *Science* 343: 379–380.
514 Satheesh, S. K., Torres, O., Remer, L. A., Babu, S. S., Vinoj, V., Eck, T. F., Kleidman, R. G. and
515 Holben, B. N. (2009). Improved assessment of aerosol absorption using OMI-MODIS joint
516 retrieval. *J. Geophys. Res. Atmos.* 114: D05209.
517 Sayer, A. M., Hsu, N. C., Bettenhausen, C. and Jeong, M.-J. (2013). Validation and uncertainty
518 estimates for MODIS Collection 6 "Deep Blue" aerosol data. *J. Geophys. Res. Atmos.* 118:
519 7864-7872.
520 Sayer, A. M., Hsu, N. C., Eck, T. F., Smirnov, A. and Holben, B. N. (2014a). AERONET-based
521 models of smoke-dominated aerosol near source regions and transported over oceans, and

implications for satellite retrievals of aerosol optical depth. *Atmos. Chem. Phys.* 14: 11493-11523.

Sayer, A. M., Munchak, L. A., Hsu, N. C., Levy, R. C., Bettenhausen, C. and Jeong, M.-J. (2014b). MODIS Collection 6 aerosol products: Comparison between Aqua's e-Deep Blue, Dark Target, and "merged" data sets, and usage recommendations. *J. Geophys. Res. Atmos.* 119: 13965-13989.

Seftor, C. J., Jaross, G., Kowitt, M., Haken, M., Li, J. and Flynn, L. E. (2014). Postlaunch performance of the Suomi National Polar-orbiting Partnership Ozone Mapping and Profiler Suite (OMPS) nadir sensors. *J. Geophys. Res. Atmos.* 119: 4413-4428.

Torres, O., Ahn, C. and Chen, Z. (2013). Improvements to the OMI near-UV aerosol algorithm using A-train CALIOP and AIRS observations. *Atmos. Meas. Tech.* 6:3257-3270.

Tsay, S.-C. et al. (2013). From BASE-ASIA toward 7-SEAS: A satellite-surface perspective of boreal spring biomass-burning aerosols and clouds in Southeast Asia. *Atmos. Environ.* 78: 20-34.

van Donkelaar, A., Martin, R. V. and Park, R. J. (2006). Estimating ground-level $PM_{2.5}$ using aerosol optical depth determined from satellite remote sensing. *J. Geophys. Res. Atmos.* 111: D21201.

539 Welton, E. J., Campbell, J. R., Spinhirne, J. D. and Scott, V. S. (2001). Global monitoring of
540 clouds and aerosols using a network of micro-pulse lidar systems, In *Lidar Remote Sensing for*
541 *Industry and Environmental Monitoring*, Singh, U. N., Itabe, T., and Sugimoto, N., (Eds.),
542 *Proc. SPIE* 4153: 151-158.
543 Welton, E. J., Voss, K. J., Gordon, H. R., Maring, H., Smirnov, A., Holben, B., Schmid, B.,
544 Livingston, J. M., Russell, P. B., Durkee, P. A., Formenti, P. and Andreae, M. (2000). Ground-
545 based lidar measurements of aerosols during ACE-2: instrument description, results, and
546 comparisons with other ground-based and airborne measurements. *Tellus B* 52: 636-651.
547 Welton, E. J., Voss, K. J., Quinn, P. K., Flatau, P. J., Markowicz, K., Campbell, J. R., Spinhirne,
548 J. D., Gordon, H. R. and Johnson, J. E. (2002). Measurements of aerosol vertical profiles and
549 otical properties during INDOEX 1999 using micropulse lidars. *J. Geophys. Res. Atmos.* 107:
550 8019.
551

552 **Table Captions**

553 **Table 1.** Ground-based instruments used in comparisons with ASHE-retrieved SSA (AERONET)
554 and aerosol heights (MPLNET). Only data in March and April are used during the data period
555 shown.

556 **Table 2.** Comparison statistics of ASHE-retrieved aerosol heights against CALIOP-derived
557 heights. The number of data points (N), mean CALIOP/ASHE heights, fraction of data within 1
558 km, root-mean-square error (RMSE), and mean bias (MB) are shown for different algorithm
559 types and QA filters.

560 **Table 3.** As table 2 except comparison statistics against MPLNET-derived aerosol heights.
561

562 **Table 1.** Ground-based instruments used in comparisons with ASHE-retrieved SSA (AERONET)
563 and aerosol heights (MPLNET). Only data in March and April are used during the data period
564 shown.

Instrument	Site name	Location (latitude, longitude, elevation)	Data period
AERONET	Chiang Mai Met Station	18.77°N, 98.97°E, 312 m	2013.03.01-2015.04.30
	Doi Ang Khang	19.93°N, 99.05°E, 1536 m	2013.03.01-2015.04.13
	Luang Namtha	20.93°N, 101.42°E, 557 m	2013.03.01-2014.04.11
	Maeson	19.83°N, 99.17°E, 502 m	2014.03.02-2014.04.22
	Omkoi	17.80°N, 98.43°E, 1120 m	2014.03.02-2015.04.19
MPLNET	Doi Ang Khang	19.93°N, 99.05°E, 1536 m	2013.03.02-2014.04.18

565

566

567 **Table 2.** Comparison statistics of ASHE-retrieved aerosol heights against CALIOP-derived
568 heights. The number of data points (N), mean CALIOP/ASHE heights, fraction of data within 1
569 km, root-mean-square error (RMSE), and mean bias (MB) are shown for different algorithm
570 types and QA filters.

Algorithm type	QA filter	N	Mean CALIOP	Mean ASHE	% within 1 km	RMSE	MB
Complete algorithm	Unfiltered	627	3.0 km	2.9 km	74%	1.1 km	-0.1 km
	All QA	335	2.9 km	2.9 km	81%	1.0 km	0.0 km
	Best QA	177	3.0 km	2.8 km	84%	0.8 km	-0.2 km
Simplified algorithm	All QA	342	2.9 km	3.0 km	61%	1.2 km	0.0 km
	Best QA	205	3.1 km	2.8 km	64%	1.1 km	-0.3 km

571

572

573 **Table 3.** As table 2 except comparison statistics against MPLNET-derived aerosol heights.

Algorithm type	QA filter	N	Mean MPLNET	Mean ASHE	% within 1km	RMSE	MB
Complete algorithm	Unfiltered	17	3.5 km	4.1 km	71%	1.7 km	0.5 km
	All QA	13	3.5 km	3.5 km	77%	1.1 km	0.1 km
	Best QA	7	3.7 km	3.6 km	71%	1.1 km	-0.1 km
Simplified algorithm	All QA	30	3.6 km	3.7 km	70%	0.9 km	0.0 km
	Best QA	16	3.8 km	3.6 km	75%	0.8 km	-0.2 km

574

575

576 **Figure Captions**

577 **Fig. 1.** Study domain and site locations of ground-based instruments. Green diamonds are
578 AERONET-only sites (from west to east: Omkoi, Chiang Mai Met Station, Maeson, Luang
579 Namtha, and Son La). The red star indicates Doi Ang Khang, which had both AERONET and
580 MPLNET instruments.

581 **Fig. 2.** Flowchart of the ASHE algorithm.

582 **Fig. 3.** Application of the ASHE algorithm to a smoke event observed on 29 March 2013. Shown
583 are (a) VIIRS RGB image with MODIS/Aqua fire mask in red dots and the location of Doi Ang
584 Khang marked with a yellow star, (b) ASHE-retrieved ATH, comparisons of (c) the retrieved
585 ATH against CALIOP-derived and (d) MPLNET-derived values, and (e) the retrieved SSA
586 against AERONET inversion data. The black lines crossing from south to north in Figs. 1(a)-1(b)
587 are the CALIOP track.

588 **Fig. 4.** Frequency distributions of SSA from ASHE (red) and AERONET (blue) over the study
589 domain in March and April from 2013 to 2015. The mean (or median) SSAs are 0.89 for both
590 data sets, standard deviations 0.030 and 0.033, and the number of data points 59 and 503 for
591 ASHE and AERONET, respectively.

592 **Fig. 5.** RMSE of the ASHE-retrieved ATHs as compared to CALIOP-derived values, and number
593 of data points remaining as a function of thresholds for three different QA filters that can affect

the retrieval accuracy: (a) number of pixels discarded at the edge of the VIIRS/OMPS swath in both cross-track directions, (b) number of collocations between VIIRS/OMPS and CALIOP for SSA retrievals, and (c) relative standard deviation (RSD) of the ratio between UVAI and AOD over the consecutive 3 × 3 pixels. Dashed lines show thresholds chosen for the QA filters.

Fig. 6. Scatterplots between CALIOP-derived and ASHE-retrieved ATHs (upper) and corresponding SSA comparisons between AERONET and ASHE (lower) for data without QA filters (left), with the edge-of-swath filter (middle), and with the number-of-collocation filter in addition to the edge-of-swath filter (right). The dashed and dotted lines show ±1.0 km and ±1.5 km interval for ATH and ±0.03 and ±0.05 for SSA, respectively. The interval for AERONET SSA shows standard deviation of the mean SSAs derived from the six AERONET sites used. The number of data points (N), MB, RMSE, and fraction of data falling within expected error (%EE) are shown. For %EE, values in parentheses indicate ±1 km and ±0.03 for ATH and SSA respectively; values not in parentheses indicate ±1.5 km and ±0.05 respectively.

Fig. 7. Time series of ASHE-retrieved and MPLNET-derived ATHs (top), VIIRS-retrieved and AERONET-observed AODs (middle), and ASHE- and AERONET-retrieved SSAs (bottom) from the complete algorithm (left) and simplified algorithm (right). Only best QA data are shown. The MPLNET and AERONET data are presented only if there are ASHE-retrieved ATH data, while

611 the gray dots represent the full MPLNET/AERONET data records. The black vertical line
612 separates data for 2013 and 2014.
613

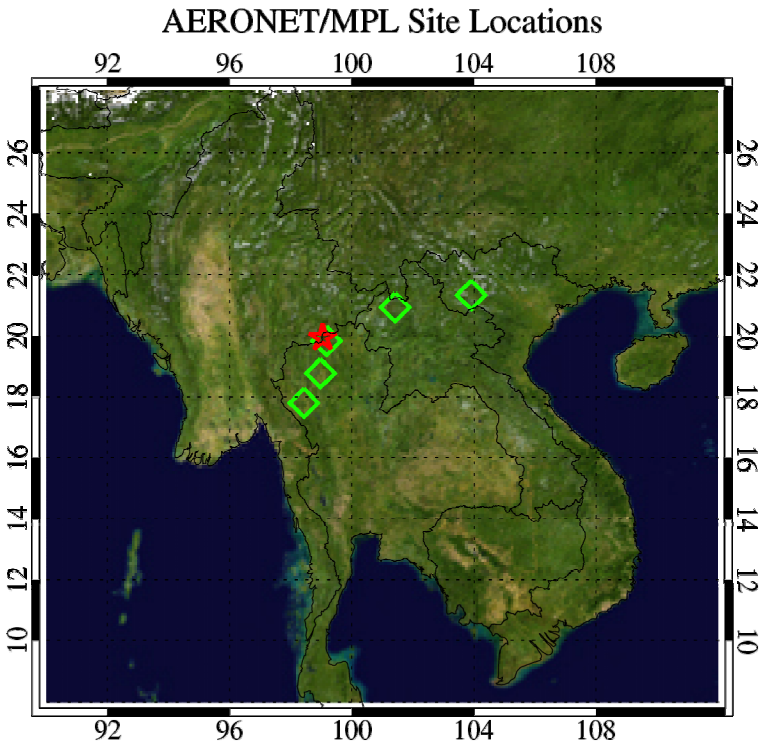

614

615 **Fig. 1.** Study domain and site locations of ground-based instruments. Green diamonds are

616 AERONET-only sites (from west to east: Omkoi, Chiang Mai Met Station, Maeson, Luang

617 Namtha, and Son La). The red star indicates Doi Ang Khang, which had both AERONET and

618 MPLNET instruments.

619

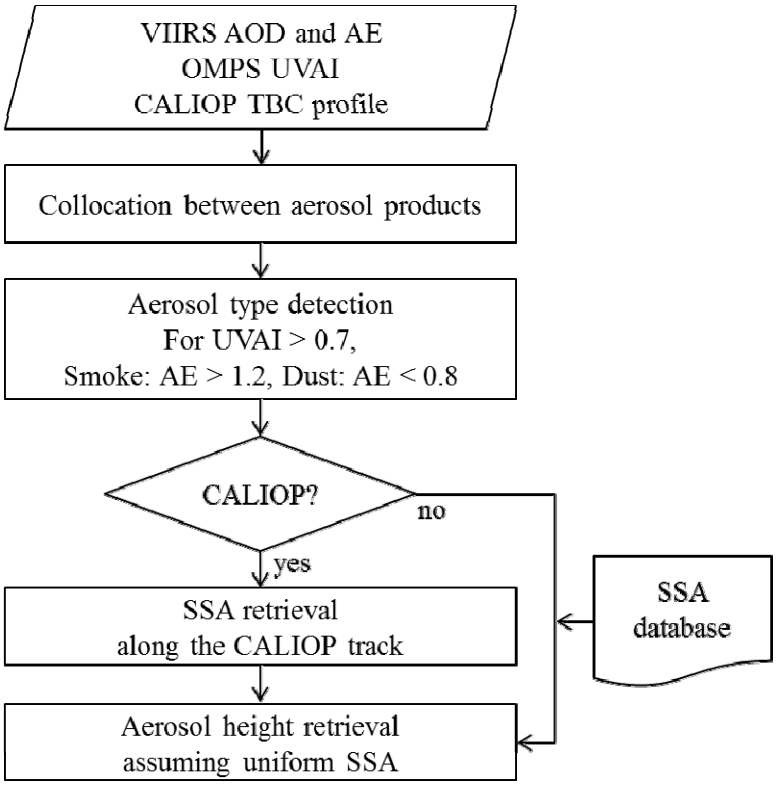

620

621 **Fig. 2.** Flowchart of the ASHE algorithm.

622

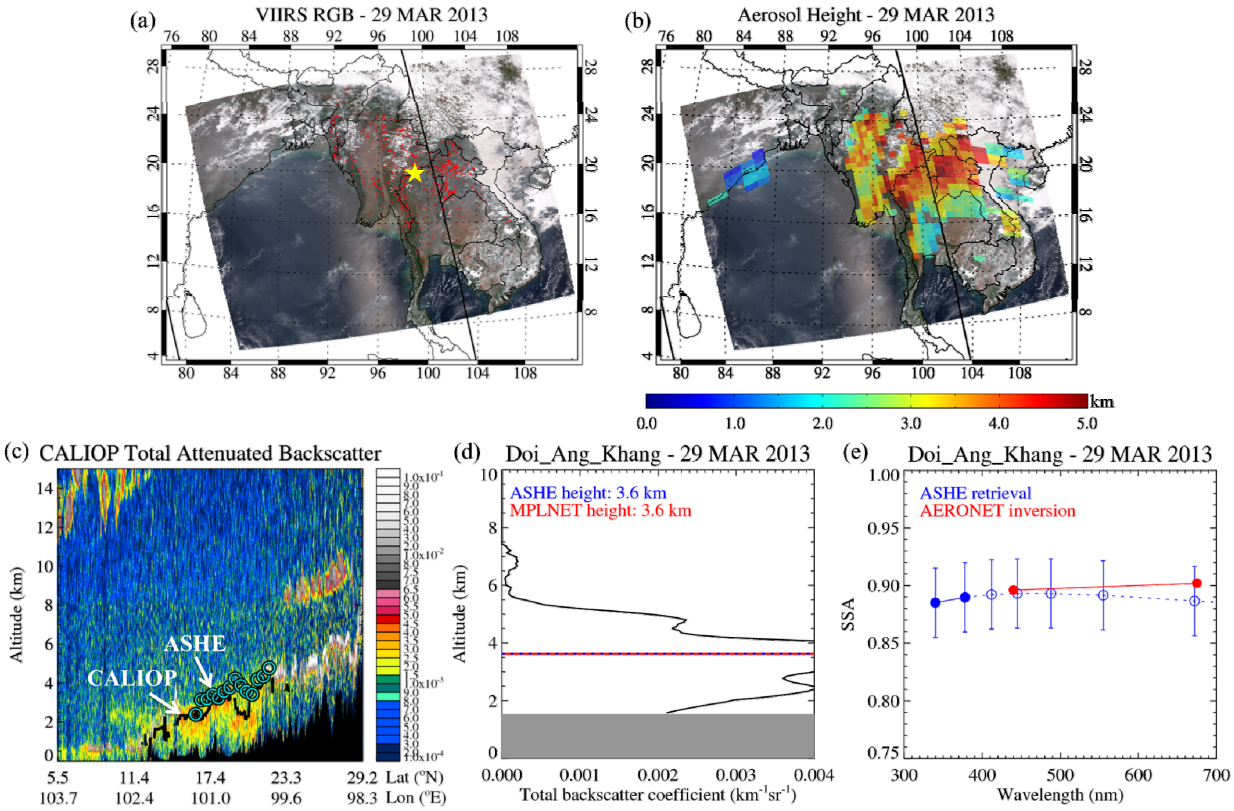

623

624 **Fig. 3.** Application of the ASHE algorithm to a smoke event observed on 29 March 2013. Shown
625 are (a) VIIRS RGB image with MODIS/Aqua fire mask in red dots and the location of Doi Ang
626 Khang marked with a yellow star, (b) ASHE-retrieved ATH, comparisons of (c) the retrieved
627 ATH against CALIOP-derived and (d) MPLNET-derived values, and (e) the retrieved SSA
628 against AERONET inversion data. The black lines crossing from south to north in Figs. 1(a)-1(b)
629 are the CALIOP track.

630

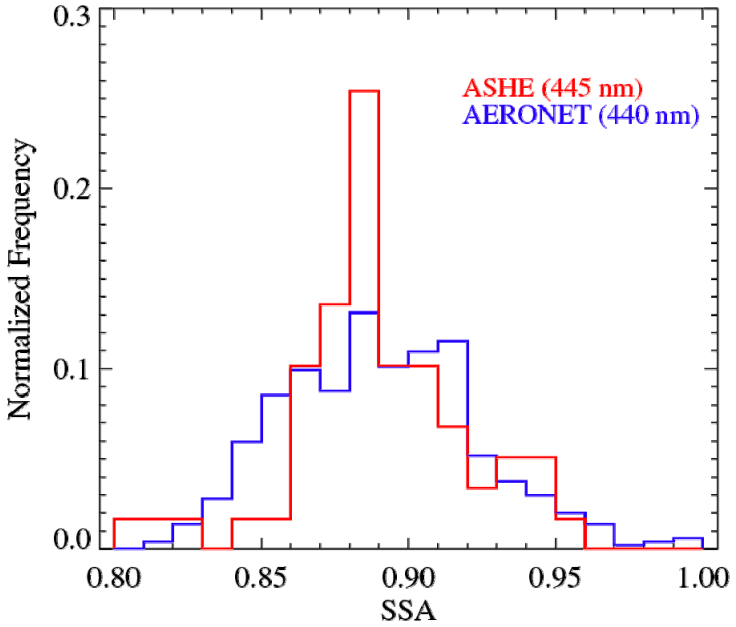

631

632 **Fig. 4.** Frequency distributions of SSA from ASHE (red) and AERONET (blue) over the study
633 domain in March and April from 2013 to 2015. The mean (or median) SSAs are 0.89 for both
634 data sets, standard deviations 0.030 and 0.033, and the number of data points 59 and 503 for
635 ASHE and AERONET, respectively.

636

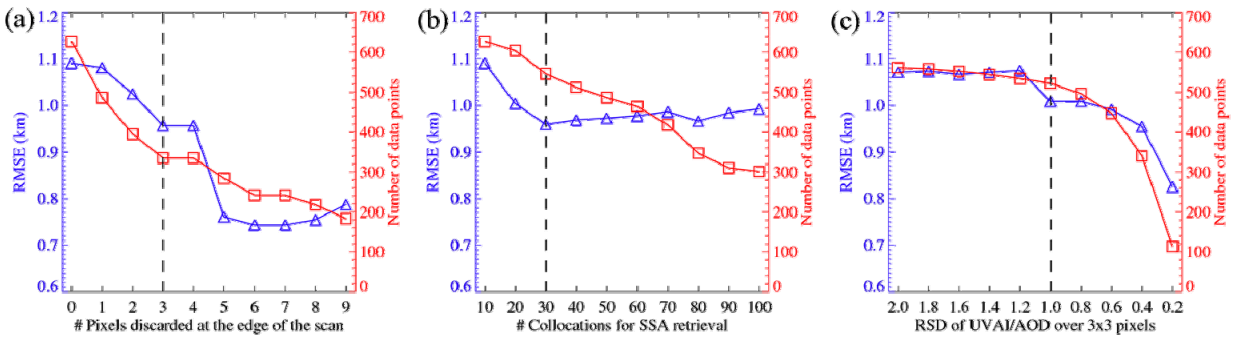

637

638 **Fig. 5.** RMSE of the ASHE-retrieved ATHs as compared to CALIOP-derived values, and number
639 of data points remaining as a function of thresholds for three different QA filters that can affect
640 the retrieval accuracy: (a) number of pixels discarded at the edge of the VIIRS/OMPS swath in
641 both cross-track directions, (b) number of collocations between VIIRS/OMPS and CALIOP for
642 SSA retrievals, and (c) relative standard deviation (RSD) of the ratio between UVAI and AOD
643 over the consecutive 3 × 3 pixels. Dashed lines show thresholds chosen for the QA filters.

644

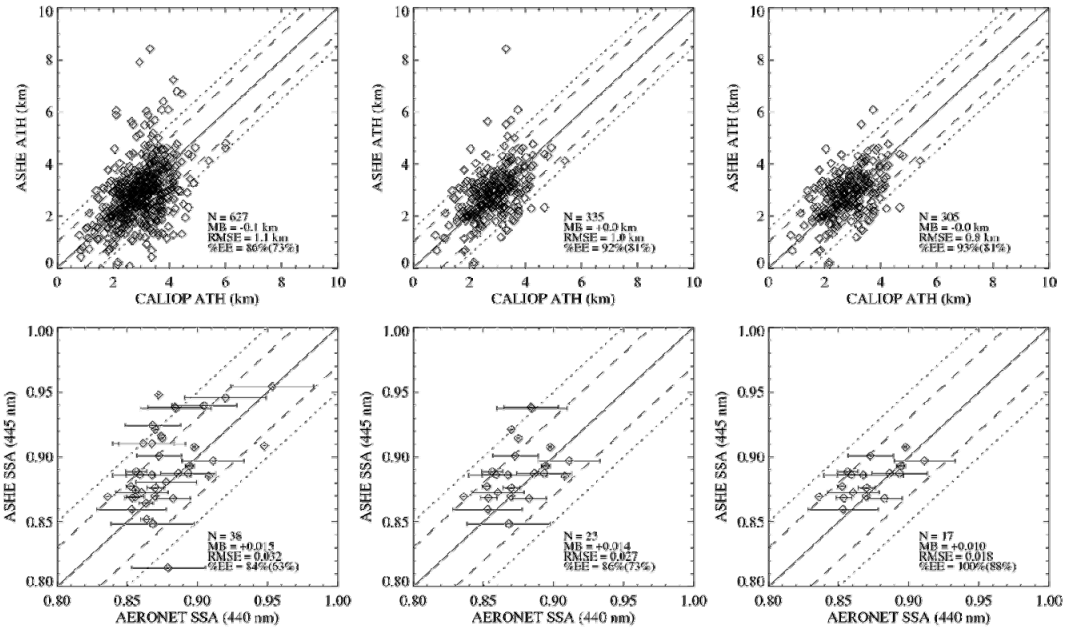

Fig. 6. Scatterplots between CALIOP-derived and ASHE-retrieved ATHs (upper) and corresponding SSA comparisons between AERONET and ASHE (lower) for data without QA filters (left), with the edge-of-swath filter (middle), and with the number-of-collocation filter in addition to the edge-of-swath filter (right). The dashed and dotted lines show ±1.0 km and ±1.5 km interval for ATH and ±0.03 and ±0.05 for SSA, respectively. The interval for AERONET SSA shows standard deviation of the mean SSAs derived from the six AERONET sites used. The number of data points (N), MB, RMSE, and fraction of data falling within expected error (%EE) are shown. For %EE, values in parentheses indicate ±1 km and ±0.03 for ATH and SSA respectively; values not in parentheses indicate ±1.5 km and ±0.05 respectively.

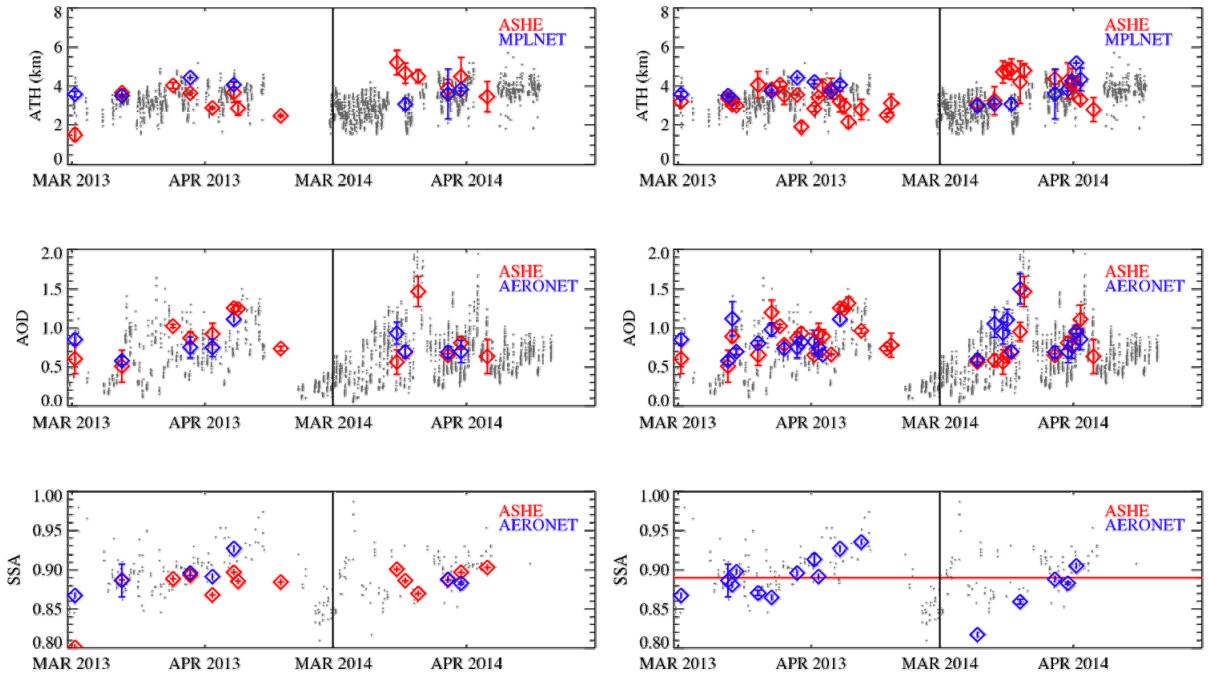

656

657 **Fig. 7.** Time series of ASHE-retrieved and MPLNET-derived ATHs (top), VIIRS-retrieved and
658 AERONET-observed AODs (middle), and ASHE- and AERONET-retrieved SSAs (bottom) from
659 the complete algorithm (left) and simplified algorithm (right). Only best QA data are shown. The
660 MPLNET and AERONET data are presented only if there are ASHE-retrieved ATH data, while
661 the gray dots represent the full MPLNET/AERONET data records. The black vertical line
662 separates data for 2013 and 2014.

663